energies

MDPI

Article

Electrothermal Model of Coupled Inductors with Nanocrystalline Cores

Kalina Detka * and Krzysztof Górecki

Department of Marine Electronics, Faculty of Electrical Engineering, Gdynia Maritime University, 81-225 Gdynia, Poland; k.gorecki@we.umg.edu.pl
* Correspondence: k.detka@we.umg.edu.pl

Abstract: The paper proposes a new electrothermal model of a coupled inductor containing a nanocrystalline core dedicated to the analysis of electrical energy conversion systems. The formulated model has a form of a subcircuit for SPICE. The model takes into account the influence of direct current, frequency, skin effect, temperature, self-heating, and mutual thermal couplings on the parameters and characteristics of the coupled inductors. The form of the developed model and the method of model parameter estimation are presented. The applied measuring system is presented. The results of measurements and calculations made with the use of the proposed model are presented and commented on.

Keywords: ferromagnetic cores; electrothermal model; nonlinear thermal model; coupled inductor; SPICE; modelling; DC–DC converters

Citation: Detka, K.; Górecki, K. Electrothermal Model of Coupled Inductors with Nanocrystalline Cores. *Energies* **2022**, *15*, 224. https://doi.org/10.3390/en15010224

Academic Editor: Bertrand Lenoir

Received: 3 December 2021
Accepted: 28 December 2021
Published: 29 December 2021

1. Introduction

The pursuit of the miniaturisation of electric energy conversion devices requires an increase in switching frequency [1,2]. The factor limiting this increase in frequency are dynamic properties of semiconductor and magnetic elements (including the inductor) contained in the mentioned devices [1,3–5]. Additionally, the increasing application requirements in the field of designing devices characterised by high watt-hour efficiency and their failure-free operation force the manufacturers of electronic components and systems to design and produce systems characterised by very high reliability [6,7].

In order to obtain a long lifetime of electronic components, an effective cooling system is indispensable. Some forced cooling systems are described in [8,9], but for magnetic devices typically free cooling systems are used.

Computer software supporting the work of designers is used to analyse the properties of electronic components and systems. One of the popular kinds of software of this type is SPICE [10]. This software can use averaged models of switch-mode power supplies [11–13]. The mentioned models allow the values of currents and voltages at steady state to be computed using fast DC analysis, instead of time-consuming transient analysis. On the other hand, such models ignore, for example, the non-linearity and inertia of semiconductor devices and the non-linear dependence L(i) of magnetic components [11].

To take into account the influence of thermal phenomena (such as self-heating and mutual thermal couplings between components of an electronic component) occurring in electronic elements on their electrical characteristics, electrothermal models are used [13–16].

In the literature, electrothermal models of semiconductor and magnetic elements are described [17–21]. However, in the case of magnetic elements, the mentioned models are limited to classic inductors (single-winding inductors) or transformers [11,22], yet there are no such models for coupled inductors.

For example, in [23], an electrothermal model of an inductor with a ferromagnetic core based on the isothermal Jiles–Atherton model is proposed. Although this model takes into

account the self-heating phenomenon, the hysteresis of the magnetisation curve, the energy losses in the core, and the windings, it is a model of an inductor with only one winding. This means that it does not take into account thermal mutual couplings in the case of a larger number of windings.

On the other hand, in [24], an electrothermal model of the inductor is proposed that takes into account the self-heating phenomenon, but only in the core. This model ignores thermal phenomena occurring in the windings, the skin effect, and the mutual thermal couplings between the windings.

The papers [11,25,26] present inductor models dedicated to operating in electrical conversion systems. The model proposed in [25] is based on matching the dependence of inductance on the direct current of the inductor using a polynomial function. However, the presented model does not take into account thermal phenomena in the considered element. The model was verified in a buck converter system.

In turn, in [11,26] a model of a classic inductor with one winding is proposed. This model takes into account thermal phenomena occurring in the inductor and thermal couplings between its components. The mentioned model also takes into account the capacity of the winding, the skin effect, and the frequency of the control signal when the inductor is operating in the electrical energy conversion system. Unfortunately, this model does not take into account the case of several windings wound on one core, the magnetic coupling between individual windings, or the thermal coupling between them.

In the model previously elaborated by the authors [27], a model of a coupled inductor dedicated to operating in electrical energy systems is proposed. However, the proposed model does not take into account the skin effect or thermal phenomena occurring in this element. Additionally, the cited paper includes an extensive description of current solutions in the field of application and modelling of the coupled inductors. In the mentioned paper, it is also noted that the T-type transformer model is generally adopted as the main model for formulating a coupled inductor model. This model is the basic model of the transformer, with the structure described in [28] containing three coils with a common node.

However, in [29], it is noticed that the T-type transformer model is asymmetric in relation to the symmetrical structure of the transformer and insufficient for the analysis of systems such as, e.g., a multi-phase DC–DC buck converter, because it has magnetising inductance only in one of the windings [30].

The analysis shows that there are no electrothermal models of coupled inductors dedicated to operating in electrical conversion systems.

This paper presents a new electrothermal model of the coupled inductors dedicated to the analysis of electrical energy conversion systems. The form of the model is described. Some results of measurements and computations confirming the usefulness of this model are also presented.

Section 2 presents the form of a new electrothermal model of coupled inductors. Section 3 describes the method of estimating the parameters of the formulated model. Section 4 discusses the element selected for the investigations and the measuring setup used. The obtained results of the measurements and the calculations are included in Section 5.

2. Model Form

In order to formulate an electronic component model, it is necessary to define the appropriate equations describing phenomena occurring in the considered element. The parameters appearing in the formulated dependences are determined from the performed measurements or from the catalogue data [27].

This section proposes a new electrothermal model of coupled inductors dedicated to the analysis of electrical energy conversion systems. This model is based on the model presented in paper [27] and represents a coupled inductor containing any number of windings n. The new model additionally takes into account the skin effect, self-heating phenomena, and mutual thermal coupling between inductor components. All the mentioned phenom-

ena were omitted in the presented model in paper [27]. Due to the simplification of the description and the improvement of its comprehensibility, the considerations are limited to the case where the coupled inductor contains three windings. The considerations were carried out for an inductor with a nanocrystalline core. The proposed model is in the form of a subcircuit for SPICE. The network representation of this model is shown in Figure 1.

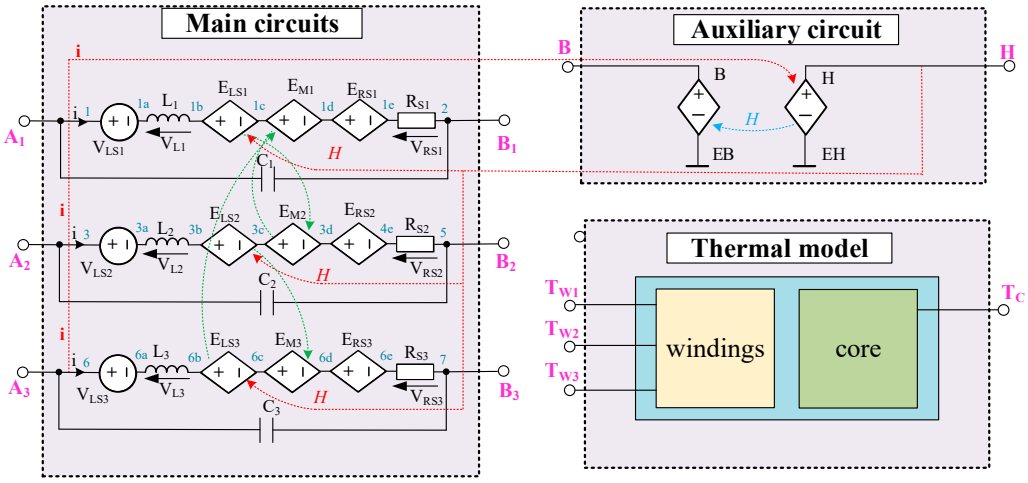

Figure 1. Network representation of an electrothermal model of a coupled inductor.

The developed model consists of three blocks: the main circuit, the auxiliary circuit, and the thermal model. The structure of the proposed model is shown in Figure 2. This model takes into account the influence of frequency, skin effect, direct current, temperature, and thermal phenomena on the characteristics of the coupled inductors.

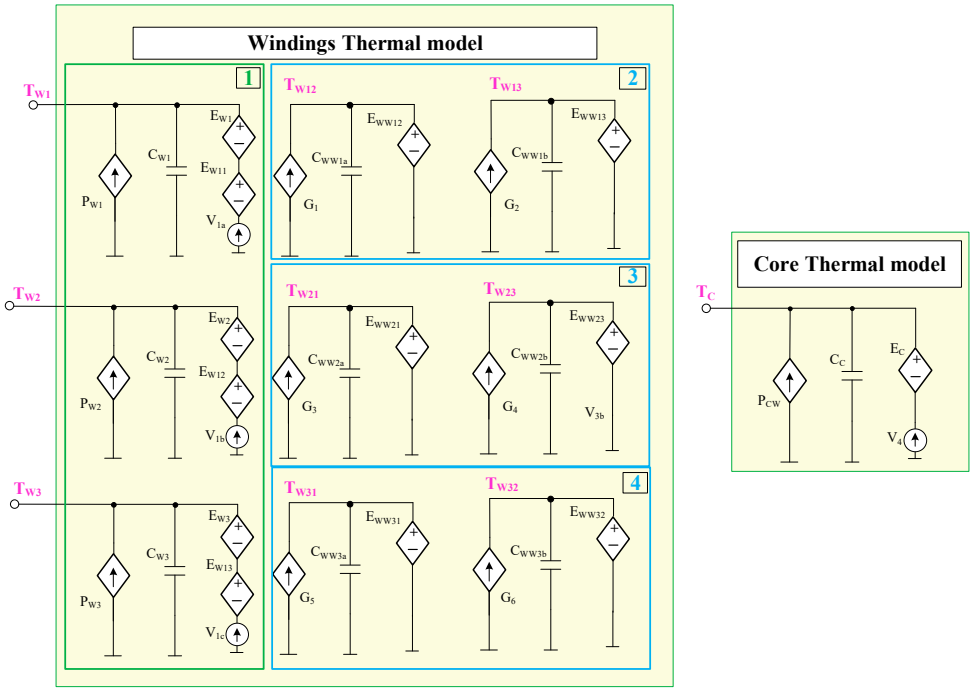

Figure 2. Network representation of the thermal model of a coupled inductor.

The main circuit describes the properties of individual windings of the modelled inductors connected between terminals A_i and B_i (i = 1 . . . n). The model of each winding consists of six series of connected elements: a voltage source with zero efficiencies V_{LSi}; a linear inductor with inductance L_i; controlled voltage sources E_{LSi}, E_{Mi}, and E_{RSi}; and a

resistor R_{Si}. The capacitor C_i, connected in parallel to the terminals A_i and B_i, represents parasitic capacitance of the winding.

The controlled voltage source E_{LSi} represents the inductance of the i-th inductor winding, and its efficiency is described by the following formula [11]:

$$E_{LSi} = a_i \cdot \frac{z_i^2 \cdot S_{Fe} \cdot B_{sat} \cdot A}{l_{Fe} \cdot (|H| + A)^2 + A \cdot B_{sat} \cdot l_p / \mu_0} \cdot \frac{V_{Li}}{L_i} \quad (1)$$

where z_i is the number of winding turns, S_{Fe} is the cross-section area of the core, B_{sat} is the saturation of the magnetic flux density, A is the field parameter, H is the magnetic force, l_{Fe} is the magnetic path length, l_p is the air gap length, a_i is the scaling factor, and V_{Li} is the voltage on a linear inductor L_i.

The controlled voltage source E_{Mi} represents the mutual inductance between the i-th winding and the other windings, expressed by the following formula [27]:

$$E_{Mi} = \sum_{\substack{j=1 \\ j \neq 1}}^{n} k_j \cdot V_{ELSj} \quad (2)$$

where k_j is the magnetic coupling coefficient, V_{ELSj} is the voltage at the source E_{LSj}, and n is the number of inductor windings.

The controlled voltage source E_{SRi} represents a voltage drop in the series resistance of the inductor as a result of the skin effect and self-heating. Its efficiency is described by the following formula [11]:

$$E_{SRi} = V_{RSi} \cdot \alpha_\rho \cdot (T_{Wi} + T_a - T_0) + \frac{l_d}{d_d} \cdot \sqrt{\mu_0 \cdot \rho \cdot (1 + \alpha_\rho \cdot (T_{Wi} + T_a - T_0))} \cdot i_{Li} \quad (3)$$

where V_{RSi} denotes the voltage on the resistor R_{Si}; d_d is the diameter of the winding wire; l_d is the length of the winding; α_p is the temperature coefficient of copper resistivity; T_{Wi}, T_a, and T_0 are the winding temperature, ambient temperature, and reference temperature, respectively; μ_0 is the magnetic permeability of the vacuum, ρ is the copper resistivity, and i_{Li} is the current flowing through the i-th inductor winding.

In turn, the resistance value of the resistor R_{Si} corresponds to the series resistance of a single winding for the direct current and temperature T_0. The value of this resistance is calculated from the classical formula

$$R_{Si} = \rho \cdot l_d / S_d \quad (4)$$

The auxiliary circuit block consists of two controlled voltage sources, EB and EH, used to determine the magnetic flux density of the core B and the magnetic force, respectively. The efficiencies of these sources are described by the dependences [31,32]

$$B = B_{sat} \cdot \frac{H}{|H| + A} \quad (5)$$

$$H = \frac{\sum_{i=1}^{n} z_i \cdot i_i}{l_{Fe} + l_p} \quad (6)$$

where i_i is the current of the i-th winding.

Due to the very narrow hysteresis loops of the considered inductor core in the model, the core losses are neglected.

In turn, the thermal model (Figure 2) is used to determine the temperature of each winding T_{W1}, T_{W2}, and T_{W3}, and the temperature of the core T_C of the coupled inductor.

This model takes into account the phenomenon of self-heating in each winding and thermal coupling between each pair of windings and between each winding and the core.

This model consists of 10 subcircuits, nine of which are included in the thermal model of the winding and one in the thermal model of the core. For better readability of the model description, the thermal model of the winding was divided into four blocks. Block 1, contained in the thermal model of the winding, includes three subcircuits for determining the temperature of the first winding T_{W1}, the second winding T_{W2}, and the third winding T_{W3}, taking into account the self-heating in each of them and mutual thermal couplings. The subcircuits included in blocks 2, 3, and 4 are used to determine a temperature rise resulting from the mutual thermal coupling between the windings. In block 2, a temperature rise in the first winding caused by heat generation in the second (T_{W12}) winding and a temperature rise in the first winding caused by heat generation in the third (T_{W13}) winding are determined. The subcircuits in block 3 make it possible to determine a temperature rise in the second winding caused by heat generation in the first winding (T_{W21}) and in the third winding (T_{W23}). On the other hand, block 3 is used to determine temperature increases in the third winding caused by heat generation in the first (T_{W31}) and second (T_{W32}) windings. The proposed thermal winding model includes nine controlled current sources. Three of them are included in block 1, where they represent the power dissipated in each winding P_{W1}, P_{W2}, and P_{W3}. The controlled current sources G_1, G_2, G_3, G_4, G_5, and G_6 included in blocks 2, 3, and 4 represent the power dissipated in the first winding P_{W1} (G_3, G_5), the second winding P_{W2} (G_1, G_6), and the third winding P_{W3} (G_2, G_4). However, the thermal model of the core contains one controlled P_{CW} current source, the efficiency of which corresponds to the sum of the power dissipated in each winding (P_{W1} + P_{W2} + P_{W3}).

The controlled voltage sources E_{W1}, E_{W2}, and E_{W3} included in the thermal model of the windings model the nonlinear thermal resistance of individual windings.

As per the literature [16,19,33,34] and the measurements made, thermal resistance is a non-linear function of temperature and the number of windings n, in which the power is dissipated.

In the considered case of coupled inductors, the efficiency of these sources is the same and described by the empirical dependence

$$E_{Wi} = w_1 \cdot {n_U}^{\alpha} \cdot R_{thW0} + R_{thW1} \cdot \exp\left(\frac{-T_W}{T_{zW}}\right) \cdot P_{Wi} \quad (7)$$

where P_{Wi} is the power dissipated in the i-th winding; T_W is the temperature of the winding in which the power is dissipated; w_1 and α are the scaling coefficients, taking into account the number of windings in which the power is dissipated; R_{thW0} is the minimum value of thermal resistance of the winding; R_{thW1} is the maximum change value of the winding thermal resistance; T_{zW} determines the slope of $R_{thW}(T_W)$; and n_U is the number of windings in which the power is simultaneously dissipated.

The controlled voltage source E_C models the nonlinear thermal resistance between the winding and the core R_{thCW}. The efficiency of this source is described by the empirical dependence

$$E_C = w_2 \cdot \exp(-{w_{22}}^{n_U}) \cdot R_{thC0} + R_{thC1} \cdot \exp\left(\frac{-T_C}{T_{zC}}\right) \cdot P_{CW} \quad (8)$$

where T_C is the core temperature; w_2 and w_{22} are the scaling coefficients, taking into account the influence of the number of windings in which the power is dissipated on mutual thermal resistance between the core and the winding; R_{thC0} is the minimum value of mutual thermal resistance between the core and the winding; R_{thC1} is the maximum change in the value of this resistance temperature; T_{zC} determines the slope of $R_{thC}(T_C)$; and P_{CW} is the power dissipated in the winding.

In turn, the controlled voltage sources E_{W11}, E_{W12}, and E_{W13} model a temperature increase in individual windings resulting from thermal couplings between individual windings. The efficiency of these sources is described by the following empirical formula:

$$E_{W11} = T_{W12} + T_{W13} \tag{9}$$

$$E_{W12} = T_{W21} + T_{W23} \tag{10}$$

$$E_{W13} = T_{W31} + T_{W32} \tag{11}$$

where T_{W12}, T_{W13}, T_{W21}, T_{W23}, T_{W31}, and T_{W32} denote the temperature rises in individual windings caused by thermal couplings, which are determined in blocks 2, 3, and 4.

The controlled voltage sources E_{WW12}, E_{WW13}, E_{WW21}, E_{WW23}, E_{WW31}, and E_{WW32} model mutual thermal resistance between the windings. The description of the efficiency of these sources for each pair of windings is the same and is described by the following empirical formula:

$$E_{WWij} = R_{thWW0} + R_{thWW1} \cdot \exp\left(\frac{-T_{Wj}}{T_{zW}}\right) \cdot i_{WWi} \tag{12}$$

where T_{W2} is the temperature of winding 2, where no power is dissipated; R_{thWW0} is the minimum value of mutual thermal resistance between the windings; R_{thW1} is the maximum change in the value of mutual thermal resistance between the windings; and i_{WWi} is the current of the source G_i.

The voltage sources V_{1a}, V_{1b}, V_{1c}, V_{2a}, and V_4 model the ambient temperature T_a.

3. Parameter Estimation of the Electrothermal Model of Coupled Inductors

The use of the electrothermal model of the coupled inductor described in Section 2 requires the determination of the parameters of this model. The parameters of the considered electrothermal model of coupled inductors can be divided into three groups:

a. Geometrical parameters of the windings (l_d, S_d, d_d, z);
b. Magnetic parameters of the core (k, B_{sat}, A, l_p, l_{Fe}, S_{Fe});
c. Thermal parameters (R_{thW}, R_{thC}, R_{thWW}, R_{thW0}, R_{thW1}, R_{thCW0}, R_{thCW1}, R_{thWW0}, R_{thWW1}, T_{ZW}, T_{ZC}, w_1, w_2, w_{22}, α).

Values of the geometrical parameters are obtained directly from the construction of the inductor.

Values of individual parameters are determined on the basis of the catalogue data available on the manufacturer's website or the measured characteristics of the inductor. While determining the value of these parameters, the local estimation method described in [35] is used. The input data for this procedure are the measured characteristics of the considered inductor using the measuring setup shown in Section 4 and the catalogue data from the manufacturer's website [36].

The thermal parameters of the inductor were measured with the use of the measurement setup presented in Section 4. For different values of the power dissipated in one winding, the temperature of the core and all the windings of the inductor were recorded. Based on the obtained measurement results, thermal resistance of the winding, mutual thermal resistance between the core and the winding, and mutual thermal resistance between the windings were determined from the classical dependence [16,33].

In turn, to determine the magnetic parameters, the method described in [35] and the measurement setup presented in Section 4 were used. It is the most popular method for measuring the hysteresis loop described in the literature, which is based on the observation and recording of the time waveforms of the current in the primary winding and the voltage waveforms on the secondary winding of a transformer with a ferromagnetic core. Waveforms H(t) and B(t) are determined indirectly using the measured current and voltage waveforms.

4. Investigated Device and Measurement Setup

In the investigations, a coupled inductor with compensation type DK3H-3352-1011-NK made by Schurter (Figure 3) was used. It contains a toroidal nanocrystalline core in the housing made of plastic of the UL 94V-0 flammability class. The dimensions of the considered coupled inductor are an external diameter of 38.3 mm, internal diameter of 25.3 mm, and height of 15.2 mm. Three windings made of enamelled copper wire with a diameter of 1.1 mm are wound on the core [36]. Each winding contains 11 turns.

Figure 3. Investigated coupled inductor.

In order to verify the correctness of the developed model, the influence of temperature and the direct winding current on the parameters of the coupled inductor were investigated.

To determine the coupled inductor parameters, the measurement setup shown in Figure 4 was used. Figure 5 shows a photo of the measurement setup used.

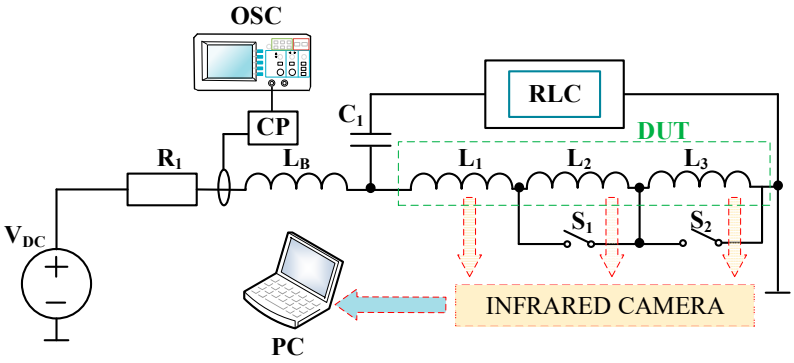

Figure 4. Setup for measuring the inductance of a coupled inductor using the LCR bridge.

Figure 5. Photo of the setup for measuring the inductance of the inductor.

In the setup presented in Figure 4, the windings of the investigated element were marked with the symbols L_1, L_2, and L_3. Depending on the position of switches S_1 and S_2, the dependence of the inductor inductance on its current was measured when the current flowed through one winding L_1, two windings L_1 and L_2, or three windings L_1, L_2, and L_3. The resistor R_1 of the resistance equal to 1 Ω limited the current of the DC voltage source V_{DC}. If the value of this current ranged from 0 to 10 A, it was measured with the multimeter UNIT-T 804. In turn, if this current exceeded 10 A it was measured using the oscilloscope (OSC) of the type RIGOL DS 1052E with the current probe (CP) of the type PINTEK PA-677.

The capacitor C_1, with a capacity of 6.7 μF, protected the RLC bridge, making a flow of the direct current through this bridge impossible. In turn, the inductor L_B, with an inductance of 1.45 mH, reduced the value of the alternating current of the voltage source V_{DC}. The automatic bridge GWINSTEK LCR-8110G [37] was used to measure the inductance of the investigated element. During the measurements, the LCR bridge worked in the mode of measurement inductance with series equivalent resistance. Additionally, by using the FLIR ETS-320 (INFRARED CAMERA) [38] infrared camera connected to a computer, the temperature distribution was recorded on all the components of the investigated inductor.

In order to ensure a reliable measurement result, it was necessary to keep the relation of $L_i >> L_B$. The L_B contained the powdered iron core (type 102 material) with 20 turns of copper wire in enamel with a diameter 2 mm. The geometric dimensions of the inductor were as follows: outer diameter of 10.3 cm, inner diameter of 5.6 cm, and height of 6.5 cm.

Figure 6 shows the measured dependence $L_B(I_{DC})$ of the blocking inductor. The measurements were made in the circuit shown in Figure 4. As a blocking inductor, a series connection of five identical inductors connected in series was used.

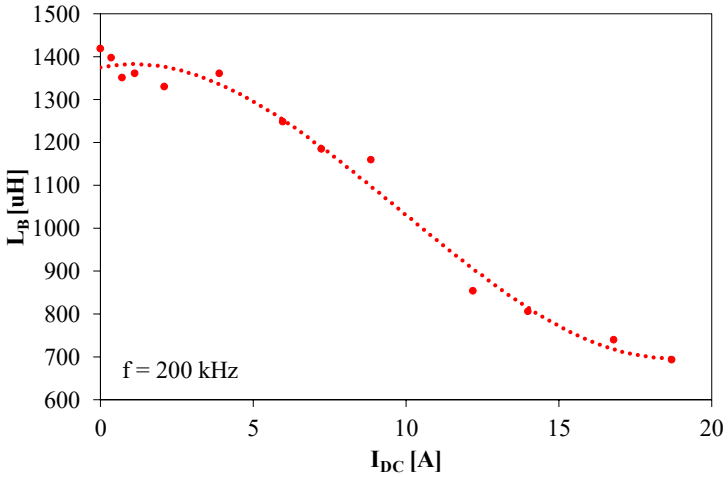

Figure 6. Dependence of the blocking inductance L_B of a blocking inductor on the direct current I_{DC}.

As can be seen in Figure 6, the dependence of inductance L_B of the blocking inductor on the direct current I_{DC} in the range of 0 to 5 A was almost constant. For I_{DC} > 5 A the inductance of the inductor decreased to the value of approx. 800 μH at I_{DC} = 19 A.

In turn, in order to characterise parameters of the nanocrystalline core of the considered coupled inductor and to determine its saturation of magnetic flux density B_{sat}, the hysteresis loop was measured using the classic measurement system shown in Figure 7 [31,32].

In the measurement setup presented in Figure 7, the JV5603P function generator was used as the source of the sinusoidal input signal V_{sin} [39]. To amplify the input signal, the AETECHRON 7228 power amplifier (PA) was used [40]. The resistor R_1 was used to limit the current flowing from the source V_{sin}, and the resistor R_2 and the capacitor C_2 represented the integrator. By recording with the RIGOL1102D [41] oscilloscope (OSC), the input current waveforms using the current probe (CP) PINTEK PA / 677 [42], and the

voltage time waveform on the capacitor C_2, the time waveform of the magnetic force from the dependence (6) was determined, and the magnetic flux density was determined from the dependence:

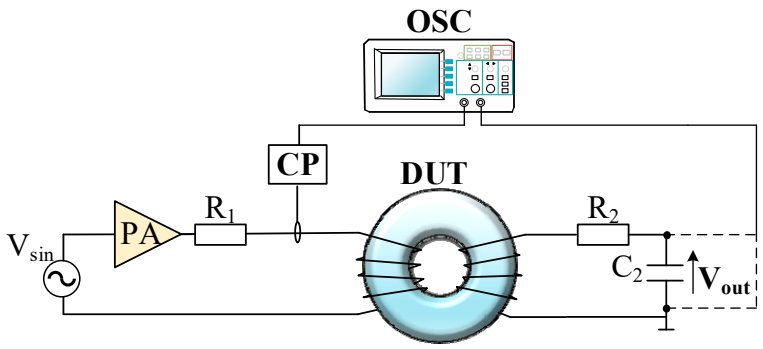

Figure 7. Setup to measure the hysteresis loop.

Figure 8 shows the hysteresis loop of the investigated nanocrystalline core obtained with the use of the measurement setup shown in Figure 7. The measurements were carried out at the input signal frequency f = 2.6 kHz. The resistance values of the resistor R_1 and R_2 were 0.5 Ω and 100 Ω, respectively, whereas the capacitance of the C_2 capacitor was equal to 3.19 μF.

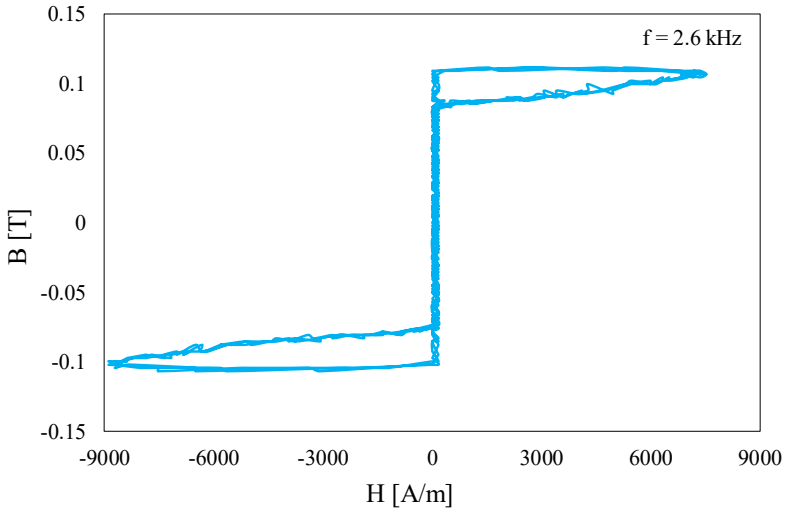

Figure 8. Hysteresis loop of the investigated nanocrystalline core.

As can be seen, the investigated core was characterised by a low value of the saturation of magnetic flux density B_{sat} equal to 110 mT and low power losses presented by a very narrow hysteresis loop.

Based on the estimation procedure described in Section 3, the values of the parameters of the electrothermal model of the investigated inductor were determined and are collected in Tables 1–3.

Table 1. Values of the geometrical parameters of the coupled inductor.

l_d (m)	S_d (m^2)	d_d (mm)	$z_1 = z_2 = z_3$
0.528	$7.85 \cdot 10^{-7}$	1	11

Table 2. Values of the magnetic parameters of the coupled inductor.

a_1	S_{Fe} (m^2)	B_{sat} (T)
7.27	$98 \cdot 10^{-6}$	0.11
A (A/m)	l_p (mm)	l_{Fe} (m)
4	4	0.102

Table 3. Values of the thermal parameters of the coupled inductor.

R_{thC0} (K/W)	R_{thC1} (K/W)	R_{thW0} (K/W)	R_{thW1} (K/W)
23	23	12.9	24
R_{thWW0} (K/W)	Rth_{WW1} (K/W)	T_{zW} (K)	T_{zC} (K)
6.4	31	21	23
w_1	w_2	w_{22}	α
0.9839	1.1675	0.164	–0.55

Tables 1–3 summarise the values of the geometric parameters, the magnetic parameters, and the thermal parameters of the electrothermal model of the coupled inductor. The model assumed that all the windings had the same value for all the parameters.

5. Results of Measurements and Calculations

In order to verify the correctness of the developed electrothermal model of coupled inductors described in Section 2, the influence of temperature, frequency, and direct current IDC on the parameters of the investigated element was examined. The measurement setup presented in Figure 4 was used to investigate the coupled inductors. The obtained measurement results were compared to the results of the calculations obtained with the use of the mentioned model. In all figures presented in this section, the principle that the points denote the measurement results and the lines illustrate the results of the calculations made with the use of the model described in Section 2 was adopted.

Additionally, in order to investigate the influence of the ambient temperature Ta on parameters of the investigated inductor, a thermostat with the considered inductor was applied to the setup shown in Figure 4. The obtained results show that the ambient temperature did not influence the inductor parameters; hence, the mentioned results are omitted in this section.

5.1. Characteristics of Coupled Inductor

Figure 9 shows the dependence of inductance L_1 of a single winding, inductances of a series connected by two windings L_{12}, and inductances of a series connected by three windings L_{123} of the coupled inductors on the direct current I_{DC} flowing through these coils at a frequency of the exciting signal equal to f = 200 kHz. The mentioned windings were wound on the same core.

The dependences $L(I_{DC})$ presented in Figure 9 show that the results of the computations performed using the proposed model fit the results of the measurements very well in all the considered connections of the windings. It is also visible that in the case when two windings were connected in series, their inductance L_{12} was over two-fold higher than inductance L_1 of the single winding. If three windings were connected in series, their inductance L_{123} was over three-fold higher than inductance L_1. All the presented dependences $L(I_{DC})$ are monotonically decreasing functions.

Figure 10 presents thermograms illustrating the temperature distribution in the investigated inductors when the current flowed through one winding (Figure 10a), two windings connected in series (Figure 10b), and three windings connected in series (Figure 10c). In each of the considered cases, the power dissipated in one winding, two series-connected windings, and three series-connected windings was equal to 2.5 W.

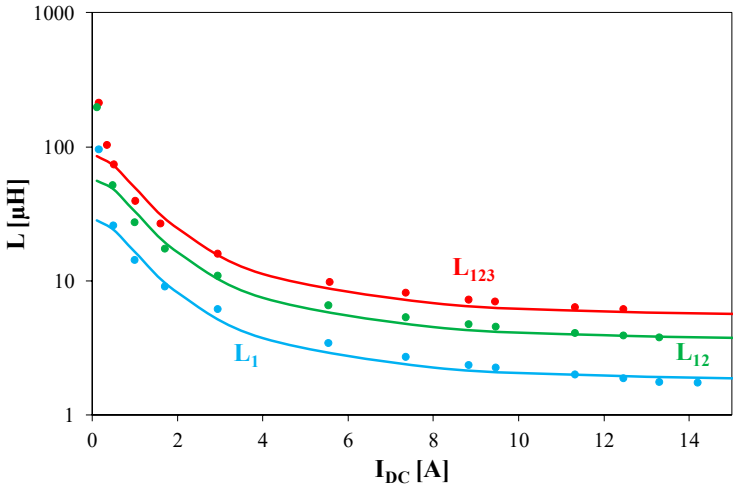

Figure 9. Dependence of inductance L_1, L_{12}, and L_{123} on the direct current I_{DC} at f = 200 kHz.

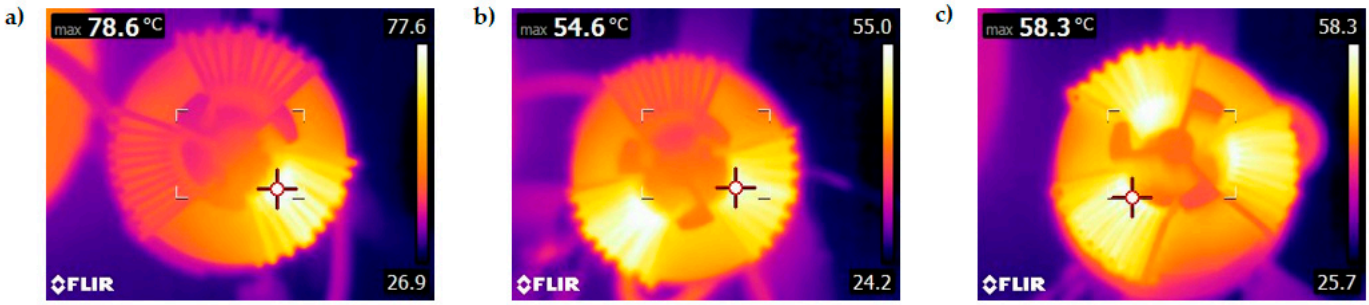

Figure 10. Thermograms illustrating the temperature distribution in the inductor when the current flows through one winding (**a**), two windings connected in series (**b**), and three windings connected in series (**c**).

It can be seen (Figure 10) that the temperature distribution of the core and the winding was uneven and depended on the number of windings through which the current flowed. It can be noticed that when the current flowed through only one winding, the temperature TW1 of that winding reached up to 78 °C, and the temperature of the T_C core, resulting from thermal couplings between the core and the winding, reached approx. 45 °C and was almost 10 °C higher than the temperature of the other windings through which no current flowed. This proves that thermal coupling between the core and the winding was stronger than between the windings. On the other hand, when the current flowed through two or three series-connected windings, the temperature of such windings T_{W12} and T_{W123} was equal to 55 and 58 °C, respectively. It was also observed that the temperature of each winding through which the current flowed was the same. Additionally, it was observed that when the current flowed through two series-connected windings, the core temperature between the windings through which the current flowed was equal to 46 °C and was almost 5 °C higher than the temperature of the core near the winding through which the current did not flow. On the other hand, when the current flowed through three series-connected windings, the core temperature between all the windings was similar and was equal to 44 °C.

Figure 11 shows the dependence of thermal resistance of a single winding R_{thW}, thermal resistance between the core and winding R_{thCW}, and the mutual thermal resistance between the windings R_{thWW} on the temperature of this winding T_{W1}.

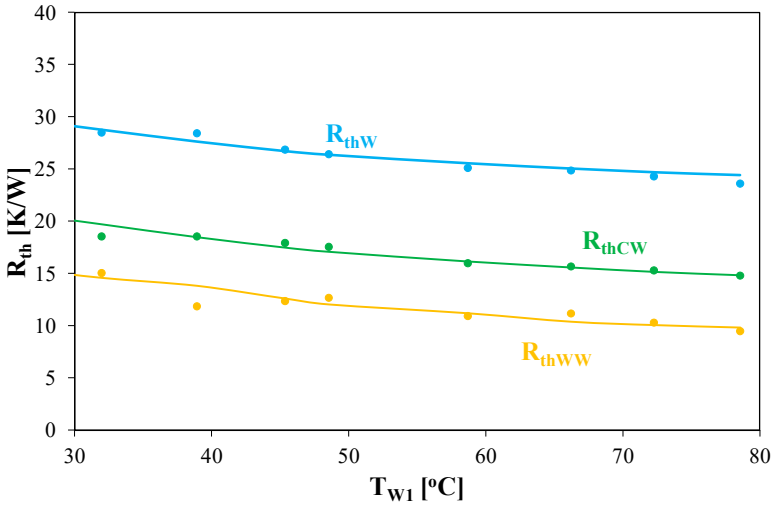

Figure 11. Dependence of thermal resistances of the inductor components on the temperature of the winding in which the power is dissipated.

As can be seen, thermal resistance of the winding R_{thW}, thermal resistance between the core and the winding R_{thCW}, and mutual thermal resistance between the windings R_{thWW} decreased with an increase in the first winding T_{W1} temperature, in which the power was dissipated. In each considered case, an increase in the winding temperature, in which the power was dissipated, of about 46 °C caused a decrease in the values of the mentioned thermal resistances by approx. 5 K/W.

Figure 12 presents the dependence of mutual thermal resistances between the core and one R_{thCW1}, two R_{thCW12}, or three $R_{thCW123}$ windings on the winding, in which the power was dissipated.

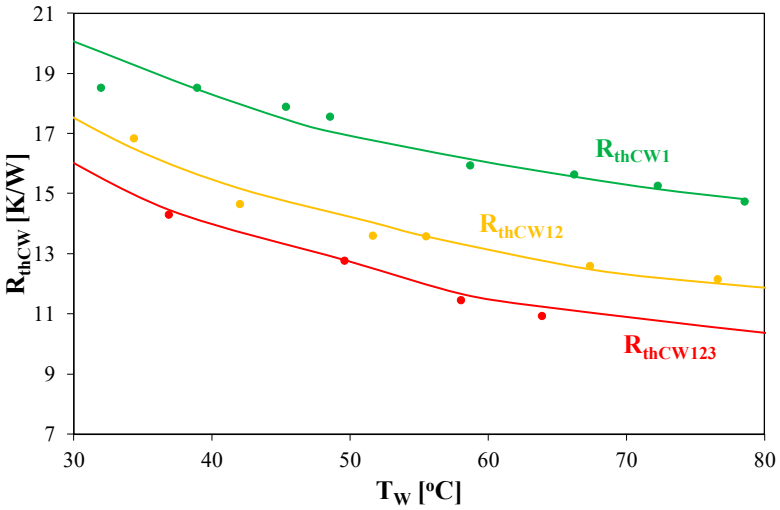

Figure 12. Dependence of mutual thermal resistance between the inductor core and the winding on the winding temperature for one, two, and three series-connected windings.

As can be seen, the number of windings in which the power was dissipated significantly influenced thermal resistance of the inductor core. An increase in the number of windings in which the power was dissipated from one to three caused a decrease in the value of thermal resistance by up to 25%.

Figure 13 shows the dependence of thermal resistance of one R_{thW1}, two R_{thW12}, and three R_{thW123} series-connected windings in which the power was dissipated on the temperature of these windings.

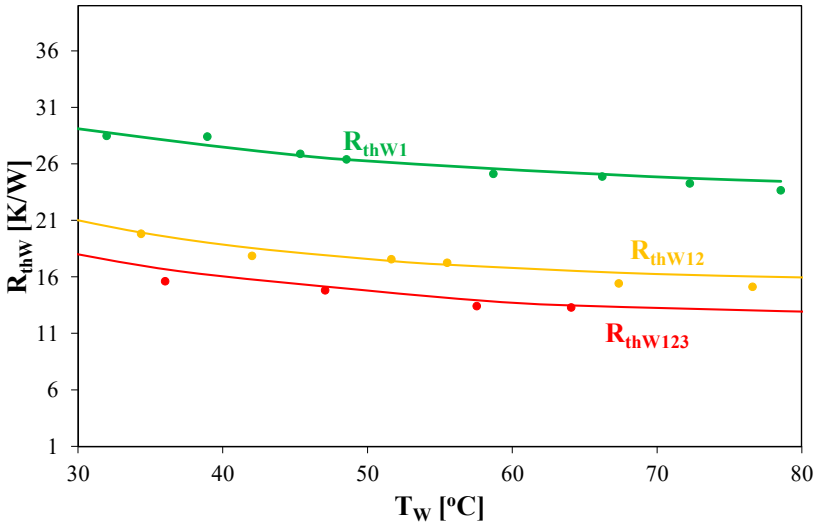

Figure 13. Dependence of thermal resistance of the inductor windings on the temperature of these windings T_{W1} with various number of powered windings at the same time.

As in the case of thermal resistance of the core, the number of windings in which the power was dissipated significantly influenced thermal resistance of the inductor winding. An increase in the number of the mentioned windings from one to three caused a decrease in the value of thermal resistance R_{thW123} of the windings by up to 70% compared to R_{thW1}.

Figure 14 shows the temperature dependence of all the inductor components on the direct current I_{DC} obtained when power was dissipated in one winding (a) and in three windings connected in series (b).

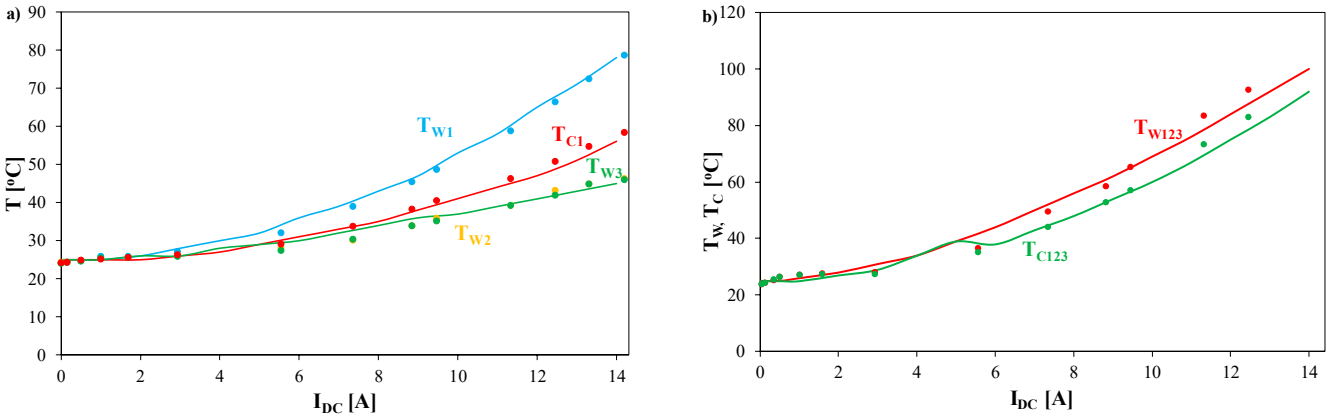

Figure 14. Dependence of the temperature of the inductor components on the direct current (**a**) when power is dissipated in one winding, (**b**) when the power is dissipated in three series-connected windings.

As can be seen in Figure 14a, an increase in the direct current flowing through one winding L1 caused an increase in the temperature of all the components of the considered inductor as a result of mutual thermal interactions between the windings. An increase in the temperature of windings T_{W2} and T_{W3} at the direct current I_{DC} = 14 A was equal to 25 °C, whereas an increase in the core temperature T_C at I_{DC} = 14 A was equal to 33 °C. On the other hand, from the dependence shown in Figure 14b, it can be seen that in the case of the power dissipated in three series-connected windings, the core and the winding temperature for I_{DC} < 6 A were the same. For I_{DC} > 6 A, the temperature of the winding was higher than the core temperature by about 10 °C.

This shows a strong thermal coupling between the components with increasing numbers of windings in which the power was dissipated. It should also be noted that the results of the calculations are in good agreement with the results of the measurements and the difference between the results of the calculations and measurements did not exceed 4%.

Figure 15 shows the dependence of the inductor core temperature on the direct current I_{DC} when the current flowed through one T_{C1} winding, two series-connected T_{C12} windings, and three series-connected T_{C123} windings.

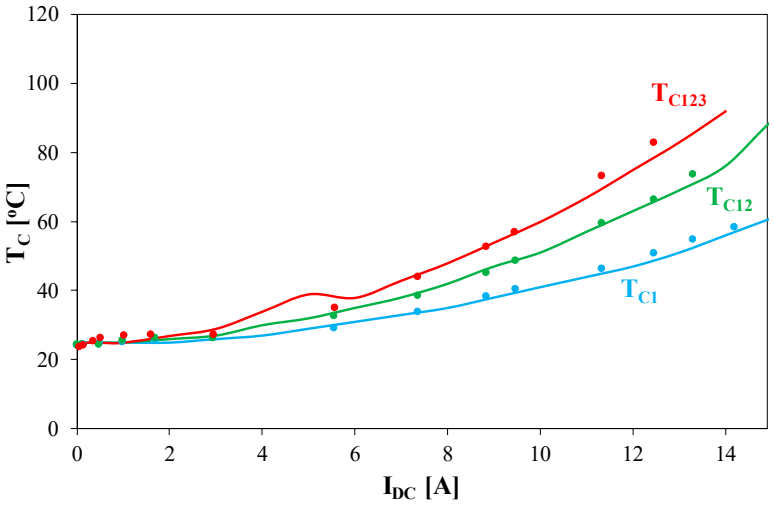

Figure 15. Dependence of the inductor core temperature on the direct current IDC when the current flows through one, two, or three windings connected in series.

As expected, an increase in the number of windings in which power was dissipated caused a rise in the core temperature. In the case when the power was dissipated in only one winding, the temperature of the core T_{C1} at I_{DC} = 14 A was equal to 59 °C. An increase in the number of windings in which the power was dissipated from one to three caused an increase in the temperature of T_{C123} to almost 100 °C. As can be seen, the increase in the temperature of the inductor core with an increase in the number windings in which the power was dissipated was non-linear, which was shown in Section 2. Additionally, it is worth noting that good agreement was obtained between the results of the calculations and measurements, and the difference between them did not exceed 5%.

Figure 16 shows the dependence of the inductor winding temperature on the direct current I_{DC} obtained when the current flowed through one T_{W1}, two series-connected windings T_{W12}, and three series-connected windings T_{W123}.

As can be seen, an increase in the number of windings in which the power was dissipated caused increases in the temperature of the inductor winding. It is observed that changes in the winding temperature with a change in the number of windings in which the power was dissipated had a non-linear character. If the current flowed through only one winding, the winding temperature at I_{DC} = 14 A was equal to 78 °C. When the current flowed through three series-connected windings, the temperature of the winding T_{W123} exceeded 100 °C. Additionally, it is worth noting that the results of the measurements and calculations are in good agreement and the difference between them did not exceed 5%.

5.2. Characteristics of Coupled Inductor

The usefulness of the proposed electrothermal model of the coupled inductor in the analysis of switching systems was verified by calculating the influence of the load resistance on the output voltage. Additionally, the influence of the load resistance on the temperature of individual components of the coupled inductor operating in the boost converter was investigated. The analysed circuit is shown in Figure 17.

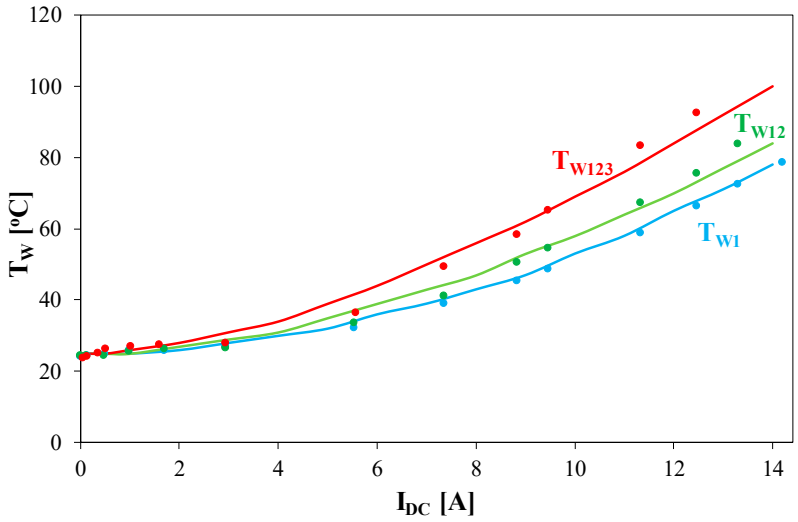

Figure 16. Dependence of the inductor winding temperature on the direct current I_{DC} flowing through one T_{W1}, two T_{W12}, or three T_{W123} windings connected in series.

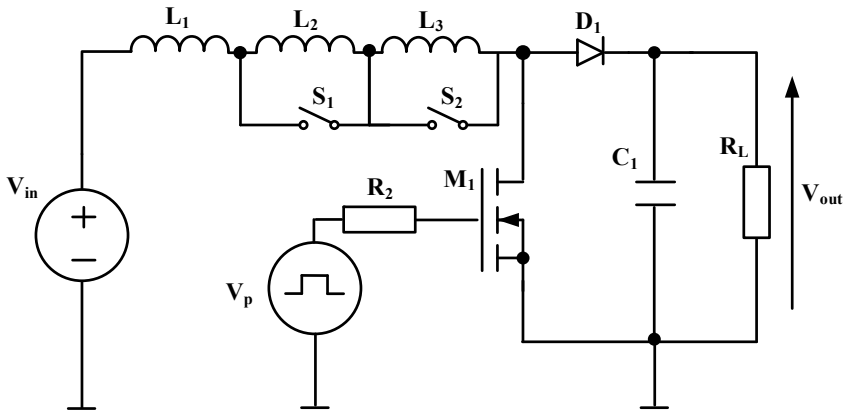

Figure 17. Analysed circuit of a boost converter.

In the considered circuit, a MOSFET transistor IRF540 (M_1), a Schottky diode 1N5822 (D_1), and passive elements R_2 = 30 Ω and C_1 = 50 µF were used. The resistor R_L is the load of the converter, and the voltage source V_{in} is the power source. The signal V_p is a square wave generator with voltage levels equal to 0 and 10 V.

Figure 18 shows the calculated dependences of the output voltage of the considered converter on load resistance at the control signal frequency f = 50 kHz, the control signal duty cycle d = 0.5, and the value of the input voltage V_{in} = 24 V. The case of the current flowing through one winding L_1, two L_{12} windings connected in series, and three L_{123} windings connected in series was considered.

As can be seen, the dependence V_{out} (R_L) had a local extreme at R_L = 20 Ω when the current flowed through only one winding. In the case of the increasing number of windings in which the power was dissipated, this extreme shifted to the left side of the considered characteristic. It is also observed that an increase in load resistance R_L from 0.1 to 10 Ω caused an almost seven-fold increase in the value of the output voltage V_{out} of the boost converter. On the other hand, at the load resistance R_L > 100 Ω, the output voltage of the boost converter was constant. Additionally, an increase in the number of windings from one to three in which the power was dissipated reduced the value of the output voltage of the considered converter by over 10%. The maximum observed at R_L equal to about 10 Ω is a result of the nonlinearity of the dependence L(i) of the inductor used. This dependence influenced the location of the border between the CCM and DCM modes.

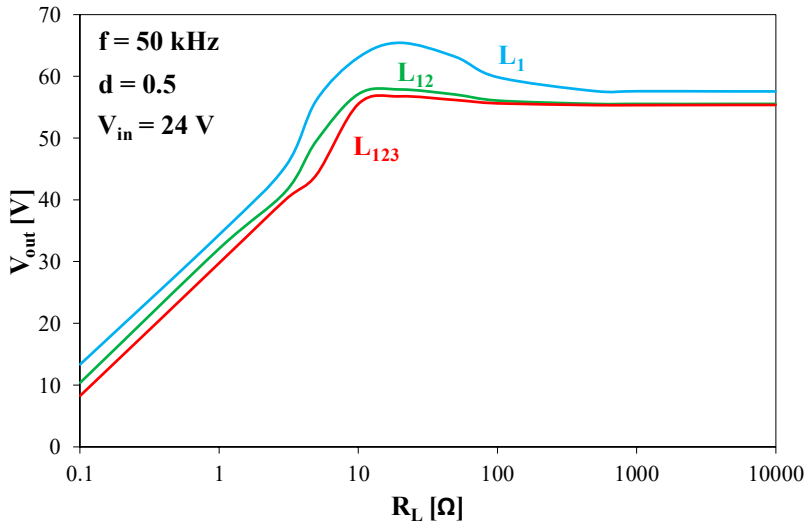

Figure 18. Dependence of the output voltage on the load resistance of the boost converter when the current flows through one coil, two coils, or three coils connected in series.

Figure 19 shows the dependence of the core temperature T_C and the winding temperature T_{W1}, T_{W2}, and T_{W3} of the coupled inductor operating in the boost converter on the load resistance. In this case, switches S_1 and S_2 were closed and the current flowed through only one coil L_1.

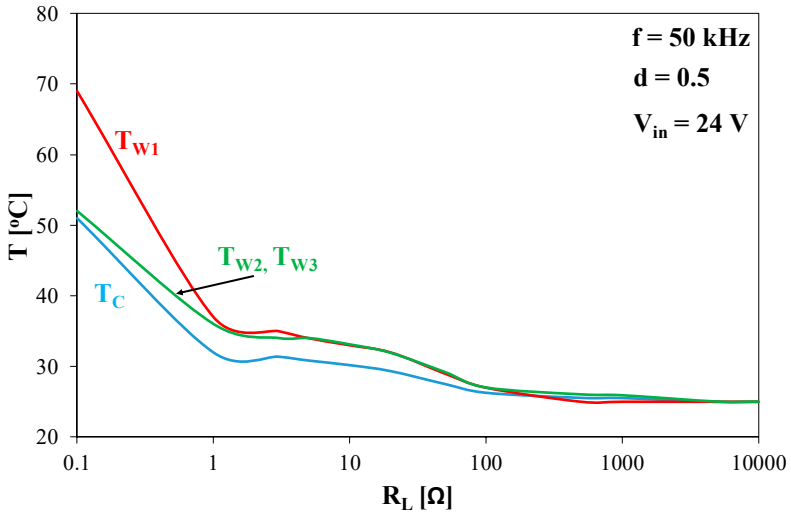

Figure 19. Dependence of the core and winding temperature on the load resistance of the boost converter when the current flows through one coil.

Figure 19 shows that an increase in the load resistance of the boost converter caused a decrease in the temperature of the core and all the windings of the coupled inductor. An increase was observed of the core temperature to T_C = 51 °C at R_L = 0.1 Ω and the temperature of the windings in which no power was dissipated at the same load resistance to T_{W1} = T_{W2} = 53 °C. This is the result of the strong thermal couplings between the windings and between the winding and the inductor core.

6. Conclusions

The paper proposes an electrothermal model of a coupled inductor with a nanocrystalline core dedicated to the SPICE software. The formulated model takes into account electrical phenomena occurring in the windings, magnetic phenomena in the core, and thermal phenomena. In contrast to the model proposed in the literature, in the proposed

model, the temperature of the core and each winding are computed. The thermal phenomena include self-heating in each of the windings and mutual thermal couplings between each pair of windings and between each winding and the inductor core.

In Table 4 some properties of the proposed model are compared with select models of the inductors presented in the paper [24,27].

Table 4. The phenomena included in the models described in the current paper and in papers [24,27].

Phenomena	New Model	Model From [24]	Model From [27]
Coupling factor	YES	NO	YES
Self-heating in the core	YES	YES	NO
Self-heating in the windings	YES	YES	NO
Thermal coupling	YES	YES	NO
Skin effect	YES	NO	NO
Number of inductor component temperatures	1 core temperature and n winding temperatures	1 temperature of the whole device	Ambient temperature only
Nonlinearity of thermal model	YES	NO	NO

The correctness of the developed model was verified experimentally for a coupled inductor containing three identical windings wound around a nanocrystalline core. The obtained results of the calculations and the measurements confirm that the developed model enabled calculations of the dependence L(i) and the temperature of the windings and the core under various conditions of supplying these windings. The differences between the obtained results of the calculations and measurements are small and did not exceed a few percent.

It has been proven that in the investigated inductor, there can be a strong variation between the temperatures of the core and the individual windings. These differences exceed as much as 20 °C. The proposed model enables the correct determination of the value of the temperature of the mentioned components of the coupled inductor, taking into account the non-uniformity of the power density generated in the investigated element and the non-linearity of the phenomena responsible for heat dissipation. The practical usefulness of the developed model for the analysis of properties of DC–DC converters was demonstrated with the example of a boost converter. The performed calculations allowed both the electrical characteristics of the considered system and the dependence of the temperature of individual components of the investigated inductor on the load resistance of the considered converter to be determined.

The formulated model can be used for the analysis of select power conversion systems. The use of this model will allow a more detailed analysis of the influence of the designed inductor to be performed on properties of this class system.

Author Contributions: Conceptualization, K.D. and K.G.; methodology, K.G. and K.D.; measurements, K.D.; computations, K.G. and K.D.; resources, K.D.; writing—original draft preparation, K.D. and K.G.; writing—review and editing, K.G. and K.D., visualization, K.G. and K.D.; supervision, K.G. All authors have read and agreed to the published version of the manuscript.

Funding: Project financed in the framework of the program by Ministry of Science and Higher Education called "Regionalna Inicjatywa Doskonałości" in the years 2019–2022, project number 006/RID/2018/19, the sum of financing 11,870,000 PLN.

Institutional Review Board Statement: Not applicable.

Informed Consent Statement: Not applicable.

Data Availability Statement: The data presented in this study are available on request from the corresponding author.

Conflicts of Interest: The authors declare no conflict of interest.

Nomenclature

Symbol	Description
A	field parameter
a_i	scaling factor
B_{sat}	saturation magnetic flux density
d_d	diameter of the wire
H	magnetic force
i_{Li}	current flowing through the i-th winding
i_{WWi}	current at the source G_i
k_j	magnetic coupling coefficient
L_i	inductance of linear inductor
l_d	length of the winding
l_{Fe}	magnetic path length
l_p	air gap length
n_u	number of windings in which the power is simultaneously dissipated
P_{CW}	power dissipated in the winding
P_{Wi}	power dissipated in the i-th winding
R_{thC0}	minimum value of mutual thermal resistance between the core and the winding
R_{thC1}	maximum change in the value of R_{thC}
R_{thW0}	minimum value of thermal resistance of the winding
R_{thW1}	maximum change in the value of mutual thermal resistance between the windings
R_{thWW0}	minimum value of mutual thermal resistance between the windings
S_{Fe}	cross-section area of the core
T_0	reference temperature
T_a	ambient temperature
T_C	core temperature
T_{Wi}	i-th winding temperature
T_{W12}, T_{W13}, T_{W21}, T_{W23}, T_{W313}, T_{W32}	temperature rises of individual windings caused by thermal couplings
T_{zC}	coefficient slope of the dependence $R_{thC}(T_C)$
T_{zW}	coefficient slope of the dependence $R_{thW}(T_W)$
V_{ELSi}	voltage on the source E_{LSj}
V_{Li}	voltage on the linear inductor L_i
V_{RSi}	voltage on the resistor R_{Si}
w_1, w_2, w_{22}	scaling coefficients taking into account the influence of the number of windings
z_i	number of turns in i-th winding
z_S	number of turns in the secondary winding
α	scaling coefficients taking into account the number of windings in which the power is dissipated
α_p	temperature coefficient of copper resistivity
μ_0	magnetic permeability of free air
ρ	copper resistivity

References

1. Barlik, R.; Nowak, M. *Energoelektronika Elementy Podzespoły Układy*; Politechnika Warszawska: Warszawa, Poland, 2014.
2. Kazimierczuk, M. *High-Frequency Magnetic Components*; Wiley: Hoboken, NJ, USA, 2014.
3. Rashid, M.H. *Power Electronic Handbook*; Academic Press: Cambridge, MA, USA; Elsevier: Amsterdam, The Netherlands, 2007.
4. Billings, K.; Morey, T. *Switch-Mode Power Supply Handbook*; McGraw-Hill: New York, NY, USA, 2011.
5. Ericson, R.; Maksimovic, D. *Fundamentals of Power Electronics*; Kluwer Academic Publisher: Norwell, MA, USA, 2001.
6. Delaux, D.; Illing, T.; El Hami, A. Reliability Climatic Test for Composite based on Probabilistic Arrhenius model. In Proceedings of the 17th IMEKO TC 10 and EUROLAB Virtual Conference: "Global Trends in Testing, Diagnostics & Inspection for 2030", Dubrovnik, Croatia, 20–22 October 2020.

7. Suhir, E.; Stamenkovic, Z. Using yield to predict long-term reliability of integrated circuits: Application of Boltzmann-Arrhenius-Zhurkov model. *Solid-State Electron.* **2020**, *164*, 107746. [CrossRef]
8. Mironova, A.; Mercorelli, P.; Zedler, A. A multi input sliding mode control for peltier cells using a cold–hot sliding surface. *J. Frankl. Inst.* **2018**, *355*, 9351–9373. [CrossRef]
9. Mironova, A.; Mercorelli, P.; Zedler, A. Robust control using sliding mode approach for ice-clamping device activated by thermoelectric coolers. *IFAC-PapersOnLine* **2016**, *49*, 470–475. [CrossRef]
10. Basso, C. *Switch-Mode Power Supply SPICE Cookbook*; McGraw-Hill: New York, NY, USA, 2001.
11. Maksimovic, D. Automatem steady-state analysis of switching power converters using a general-purpose simulation tool. In Proceedings of the IEEE Power Electronics Specialists Conference PESC, St. Louis, MO, USA, 27–27 June 1997; Volume 2, pp. 1352–1358.
12. Ben-Yaakov, S.; Adar, D. Average models as tools for studying the dynamics of switch mode DC—DC converters. In Proceedings of the 25th IEEE Power Electronics Specialists Conference—PESC'94, Taipei, Taiwan, 20–25 June 1994; Volume 2, pp. 1369–1376. [CrossRef]
13. Górecki, K.; Detka, K. Application of average electrothermal models in the SPICE-aided analysis of boost converters. *IEEE Trans. Ind. Electron.* **2019**, *66*, 2746–2755. [CrossRef]
14. Górecki, K.; Zarębski, J. Electrothermal analysis of the self-excited push-pull dc-dc converter. *Microelectron. Reliab.* **2009**, *49*, 424–430. [CrossRef]
15. Pushpakaran, B.N.; Bayne, S.B. *Modeling and Electrothermal Simulation of SiC Power Devices*; World Scientific Publishing Co Pte Ltd.: Singapore, 2019.
16. Górecki, K.; Detka, K.; Górski, K. Compact thermal model of pulse transformer taking into account nonlinearity of heat transfer. *Energies* **2020**, *13*, 2766. [CrossRef]
17. Hefner, A.R.; Blackburn, D.L. Simulating the Dynamic Electrothermal Behavior of Power Electronic Circuits and Systems. *IEEE Trans. Power Electron.* **1993**, *8*, 376–385. [CrossRef]
18. Hernandez, L.; Claudio-Sanchez, A.; Cotorogea, M.; Aguayo, J.; Rodriguez, M. 4H-SiC PiN Diode Electrothermal Model for Conduction and Reverse Breakdown for Pspice Simulator. In Proceedings of the 2008 11th IEEE International Power Electronics Congress, Cuernavaca, Mexico, 24–27 August 2008; pp. 192–197. [CrossRef]
19. Janke, W.; Hapka, A. Nonlinear thermal characteristics of silicon carbide devices. *Mater. Sci. Eng. B* **2011**, *176*, 289–292. [CrossRef]
20. Maxim, A.; Andreu, D.; Boucher, J. SPICE electrothermal modeling of power integrated circuits. In Proceedings of the 21st International Conference on Microelectronics, Nis, Yugoslavia, 14–17 September 1997. [CrossRef]
21. Zubert, M.; Starzak, L.; Jablonski, G.; Napieralska, M.; Janicki, M.; Pozniak, T.; Napieralski, A. An accurate electro-thermal model for merged SiC PiN Schottky diodes. *Microelectron. J.* **2012**, *43*, 312–320. [CrossRef]
22. Górecki, K.; Godlewska, M. Modelling characteristics of the impulse transformer in a wide frequency range. *Int. J. Circuit Theory Appl.* **2020**, *48*, 750–761. [CrossRef]
23. Górecki, K.; Detka, K. Electrothermal model of choking-coils for the analysis of dc–dc converters. *Mater. Sci. Eng. B* **2012**, *177*, 1248–1253. [CrossRef]
24. Wilson, P.R.; Ross, J.N.; Brown, A.D. Simulation of magnetics components models in electrics circuits including dynamic thermal effects. *IEEE Trans. Power Electr.* **2002**, *17*, 55–65. [CrossRef]
25. Lullo, G.; Sciere, D.; Vitale, G. Non-linear inductor modelling for a DC/DC Buck converter. In Proceedings of the International Conference on Renewable Energies and Power Quality (ICREPQ'17), Malaga, Spain, 21–25 March 2017. [CrossRef]
26. Górecki, K.; Zarębski, J.; Detka, K. Application of electrothermal average inductor model for analyses of boost converters. In Proceedings of the 22nd International Conference on Mixed Design of Integrated Circuits & Systems (MIXDES), Torun, Poland, 25–27 June 2015; pp. 417–421. [CrossRef]
27. Detka, K.; Górecki, K.; Grzejszczak, P.; Barlik, R. Modeling and Measurements of Properties of Coupled Inductors. *Energies* **2021**, *14*, 4088. [CrossRef]
28. Li, J.; Sullivan, C.R.; Schultz, A. Coupled-inductor design optimization for fast-response low-voltage dc-dc converters. In Proceedings of the IEEE Applied Power Electronics Conference, Dallas, TX, USA, 10–14 March 2002; pp. 817–823. [CrossRef]
29. Maksimovic, D.; Stankovic, A.M.; Thottuvelil, V.J.; Verghese, G.C. Modeling and simulation of power electronic converters. *Proc. IEEE* **2001**, *89*, 898–912. [CrossRef]
30. Zhu, G.; Wand, K. Modeling and Design Consideration of Coupled Inductor Converters. In Proceedings of the 2010 Twenty-Fifth Annual IEEE Applied Power Electronics Conference and Exposition (APEC), Palm Springs, CA, USA, 21–25 February 2010. [CrossRef]
31. Detka, K.; Górecki, K. Nowa metoda pomiaru krzywej magnesowania rdzenia dławika. *Prz. Elektrotechniczny* **2020**, *96*, 166–168. [CrossRef]
32. Tumański, S. *Handbook of Magnetic Measurements*; Taylor and Francis Group: Boca Raton, FL, USA, 2011.
33. Bahman, A.; Ma, K.; Blaabjerg, F. A lumped thermal model including thermal coupling and thermal boundary conditions for high power IGBT modules. *IEEE Trans. Power Electron.* **2018**, *33*, 2518–2530. [CrossRef]
34. Górecki, K.; Górecki, P. Non-linear compact thermal model of the IGBT dedicated to SPICE. *IEEE Trans. Power Electron.* **2020**, *35*, 13420–13428. [CrossRef]

35. Górecki, K.; Rogalska, M.; Zarębski, J. Parameter estimation of the electrothermal model of the ferromagnetic core. *Microelectron. Reliab.* **2014**, *54*, 978–984. [CrossRef]
36. Manufacturer's Catalog Note of Coupled Inductor. Available online: https://www.schurter.com/en/datasheet/typ_DKIH-3.pdf (accessed on 19 November 2021).
37. GWINSTEK LCR Meter Product Information. Available online: https://www.gwinstek.com/en-global/products/downloadSeriesDownNew/10096/742 (accessed on 19 November 2021).
38. Flir Product Information. Available online: https://www.flir.com/globalassets/imported-assets/document/flir-ets320-user-manual.pdf (accessed on 19 November 2021).
39. Function Generator Product Information. Available online: https://ndn.com.pl/pl/index.php?controller=attachment&id_attachment=1536 (accessed on 19 November 2021).
40. Amplfier Product Information. Available online: https://www.google.com/url?sa=t&rct=j&q=&esrc=s&source=web&cd=&ved=2ahUKEwjww5msjqT0AhXRgf0HHRyIBPEQFnoECAoQAQ&url=https%3A%2F%2Faetechron.com%2Fpdf%2F7228_OperatorManual.pdf&usg=AOvVaw2IkoWsZhqVKzmG3-lpASft (accessed on 19 November 2021).
41. Osciloscope Rigol Product Information. Available online: https://www.rigolna.com/products/digital-oscilloscopes/1000/ (accessed on 19 November 2021).
42. Pintek Current Probe Product Information. Available online: http://www.pintek.com.tw/files/pintek/PA-677-front.pdf (accessed on 19 November 2021).